SCIENCE CHINA
Life Sciences

•RESEARCH PAPER•

https://doi.org/10.1007/s11427-021-1994-1

Development of MEMS directed evolution strategy for multiplied throughput and convergent evolution of cytochrome P450 enzymes

Li Ma[1], Fengwei Li[1], Xingwang Zhang[1,2], Hui Chen[3], Qian Huang[4], Jing Su[5], Xiaohui Liu[1], Tianjian Sun[1], Bo Fang[1], Kun Liu[1], Dandan Tang[1], Dalei Wu[1], Wei Zhang[1], Lei Du[1] & Shengying Li[1,2*]

[1]*State Key Laboratory of Microbial Technology, Shandong University, Qingdao 266237, China;*
[2]*Laboratory for Marine Biology and Biotechnology, Qingdao National Laboratory for Marine Science and Technology, Qingdao 266237, China;*
[3]*Shandong Provincial Key Laboratory of Synthetic Biology, Qingdao Institute of Bioenergy and Bioprocess Technology, Chinese Academy of Sciences, Qingdao 266101, China;*
[4]*College of Life Sciences, Yantai University, Yantai 264005, China;*
[5]*State Key Laboratory of Biobased Material and Green Papermaking, Qilu University of Technology (Shandong Academy of Sciences), Jinan 250353, China*

Received May 27, 2021; accepted August 16, 2021; published online August 31, 2021

Directed evolution (DE) inspired by natural evolution (NE) has been achieving tremendous successes in protein/enzyme engineering. However, the conventional "one-protein-for-one-task" DE cannot match the "multi-proteins-for-multi-tasks" NE in terms of screening throughput and efficiency, thus often failing to meet the fast-growing demands for biocatalysts with desired properties. In this study, we design a novel "multi-enzymes-for-multi-substrates" (MEMS) DE model and establish the proof-of-concept by running a NE-mimicking and higher-throughput screening on the basis of "two-P450s-against-seven-substrates" (2P×7S) in one pot. With the multiplied throughput and improved hit rate, we witness a series of convergent evolution events of the two archetypal cytochrome P450 enzymes (P450 BM3 and P450cam) in laboratory. It is anticipated that the new strategy of MEMS DE will find broader application for a larger repertoire of enzymes in the future. Furthermore, structural and substrate docking analysis of the two functionally convergent P450 variants provide important insights into how distinct P450 active-sites can reach a common catalytic goal.

MEMS directed evolution, cytochrome P450 enzymes, high-throughput screening, convergent evolution, ambroxide 3*β*-hydroxylase

Citation: Ma, L., Li, F., Zhang, X., Chen, H., Huang, Q., Su, J., Liu, X., Sun, T., Fang, B., Liu, K., et al. (2021). Development of MEMS directed evolution strategy for multiplied throughput and convergent evolution of cytochrome P450 enzymes. Sci China Life Sci 64, https://doi.org/10.1007/s11427-021-1994-1

INTRODUCTION

Ubiquitous cytochrome P450 enzymes (P450s) are a superfamily of heme-thiolate proteins that catalyze a myriad of oxidative reactions in nature (Ortiz de Montellano, 2015). Since the natural functional diversity is believed to be an indicator of a protein family's evolvability, functionally versatile P450s have become a model system of directed evolution (DE) (Arnold et al., 2001; Jung et al., 2011; Romero and Arnold, 2009), a powerful biotechnology that won Nobel Prize in Chemistry in 2018. In past decades, significant successes have been achieved in engineering the

*Corresponding author (email: lishengying@sdu.edu.cn)

stability, catalytic efficiency, substrate scope, regio- and stereoselectivity, and even novel abiological activities of P450s using diverse DE strategies (Guengerich et al., 2009; Prier et al., 2017; Xu et al., 2020; Zhang et al., 2019; Zhou et al., 2019).

In general, a reliable, robust and cost-effective high-throughput screening (HTS) assay for fast identifying the mutant(s) with desired properties from a tremendous number of protein variants is crucial for success of any DE campaigns. Thus, many substrate- or product-based colorimetric/fluorometric assays for P450 DE screenings have been developed. For example, the *p*-nitrothiophenolate assay for detection of styrene oxide (Tee and Schwaneberg, 2006), the 4-(*p*-nitrobenzyl)pyridine assay to monitor alkene epoxidation (Alcalde et al., 2004), the 4-aminoantipyrine assay for phenolic compound detection (Wong et al., 2005), the purpald assay for evaluation of the P450 demethylation activity (Zhang et al., 2014), and the UV-vis spectrophotometric screening assay to detect indole alkylation (Brandenberg et al., 2019). However, these methods are often inapplicable because the P450 substrates and products are not always colored or fluorescent. To address this issue, NAD(P)H deletion assay has been established to screen the P450 activities in an indirect manner by monitoring the consumption of NAD(P)H, the cofactor required by most of P450s, at the absorption maximum wavelength of 340 nm (Glieder and Meinhold, 2003). However, the NAD(P)H consumption rates are not necessarily proportional to the product formation due to spontaneous oxidation and the uncoupling of P450 catalysis (Morlock et al., 2018). False positives in this kind of indirect assay are almost always observed and the hit mutants need to be rescreened. Thus, the gas chromatography/liquid chromatography (GC/LC)-mass spectrometry (MS)-based assays remain to be the universal and highly sensitive analytical approaches to screen CYP activities (Urban et al., 2014). However, these methods require expensive instruments and the costly screenings also suffer from low efficiency.

Nowadays, P450s with desired properties are increasingly demanded because of their broad application in bioproduction of diverse pharmaceuticals, natural products and industrial chemicals (Li et al., 2020). However, the current DE approaches as described above cannot generate sufficient high-quality P450 biocatalysts to meet the fast-growing demands, thus requiring development of new DE strategies with higher screening efficiency and hit rate (Markel et al., 2020; Zeymer and Hilvert, 2018).

Compared with DE that normally starts with a single parental protein and ends up with a "winner" mutant with desired properties ("one-protein-for-one-task") after rounds of screenings (Figure 1A), natural evolution (NE) targets multiple proteins for multiple tasks simultaneously (Figure 1B), and the overall outcome is a fitter organism with a set of mutant proteins that survives better and reproduces faster under given selection pressure due to the better completed tasks. Apparently, the screening throughput/efficiency of the "multi-proteins-for-multi-tasks" NE is higher than the "one-protein-for-one-task" DE. Of note, several previous reports have preliminarily demonstrated the benefits of pooling multiple substrates for improving the efficiency of the HTS assays for one P450 enzyme ("one-protein-for-multi-tasks") (Zhang et al., 2011; Zhang et al., 2012). In addition, the strategy of making substrates cocktail was applied to fast assessing P450 inhibitors as drug candidates (Chen et al., 2016). Inspired by these studies and NE, in this study, we designed and tested a novel "multi-enzymes-for-multi-substrates" (MEMS) DE model (Figure 1C) to mimic NE in principle for higher-throughput screening. As a result, active mutants were readily obtained for a majority of substrates through running a pilot MEMS DE approach on the basis of "two-P450s-against-seven-substrates" (2P×7S). With this new strategy, we witnessed a series of convergent evolution events in laboratory during MEMS DE.

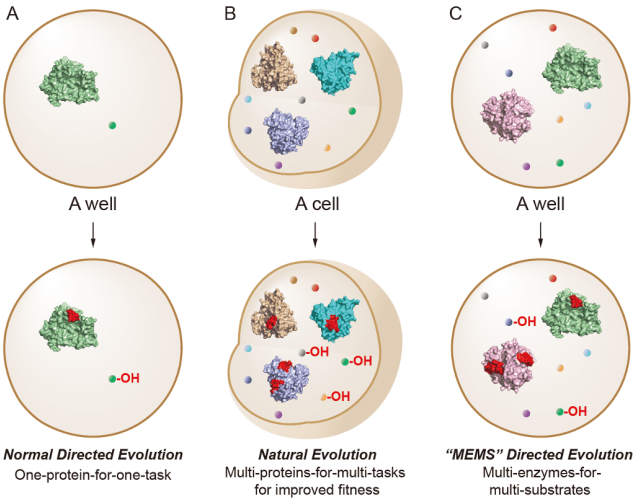

Figure 1 Schematic models of normal directed evolution (A), natural evolution (B), and "MEMS" directed evolution (C).

RESULTS

Design of the MEMS (2P×7S) DE strategy

P450 BM3 (CYP102A1) from *Bacillus megaterium* is a bacterial fatty acid hydroxylase consisting of a P450 domain naturally fused to a mammalian-like diflavin NADPH P450 reductase domain. P450 BM3 is a preferred candidate for P450-based biocatalysis because of its superb catalytic efficiency (turnover number: ~200 s^{-1} towards fatty acid substrates) and self-sufficiency (i.e., the P450 activity is independent of separate redox partner proteins) (Narhi and Fulco, 1987). P450cam (CYP101A1) from *Pseudomonas putida* catalyzes the regio- and stereospecific hydroxylation

of (+)-camphor (**1**) to form 5-*exo*-hydroxycamphor (**1a**) when supported by its innate redox partners putidaredoxin (Pdx) and putidaredoxin reductase (PdR) (Gunsalus and Wagner, 1978) (Figure 1 and Figure S1 in Supporting Information). Both enzymes have long served as the archetypal models of P450s due to their early discovery, availability of extensive structural information, and the most abundant mechanistic and mutational studies (Ahalawat and Mondal, 2018; Follmer et al., 2018; Myers et al., 2013; Poulos et al., 1987; Wang et al., 2015; Whitehouse et al., 2012). Notably, the two P450s only share a 17.2% sequence identity at the protein level (Figure S2 in Supporting Information) and the root-mean-square deviation (RMSD) of their three-dimensional structures is 11.67 (Figure S3 in Supporting Information), indicative of their distant evolutionary relationship. Unsurprisingly, their catalytic properties (i.e., catalytic efficiency, redox partner dependency, substrate specificity, and active site architecture) are distinct from each other. In this study, we chose these two intensively studied P450s to build the MEMS (2P×7S) DE model, in which the seven selected substrates included **1**, *R*-(+)-limonene (**2**), geraniol (**3**), (+)-valencene (**4**), (−)-ambroxide (**5**), taxadiene (**6**) and indole (**7**) (Figure 2).

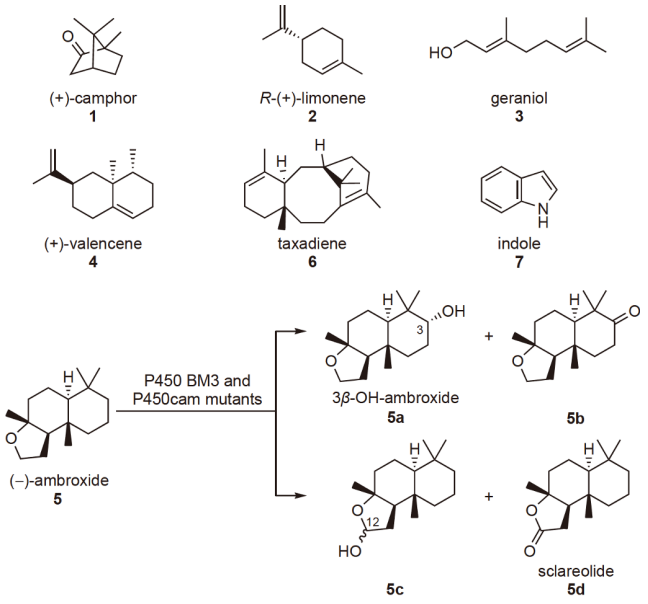

Figure 2 The P450 substrates (**1**–**7**) used in this study and the oxidative tailoring reactions of (−)-ambroxide (**5**).

P450 mutant library construction

To generate P450 mutants for screening, we elected to use the strategy of combinatorial active-site saturation test (CAST) (Reetz and Carballeira, 2007) for both P450 BM3 (the F87A mutant of P450 BM3 with an expanded active site and hence substrate scope was actually used as the starting enzyme (Whitehouse et al., 2012); this mutant will be called P450 BM3* for convenience) and P450cam. Based on analysis of the crystal structures of P450 BM3 in complex with a substrate analogue *N*-palmitoylglycine (PDB ID code: 1JPZ) (Haines et al., 2001) and of P450cam with the native substrate **1** bound (PDB ID code: 2ZWU) (Sakurai et al., 2009), the eleven active-site residues of P450 BM3* were grouped into six sites, including A site (L75 and V78), B site (F81 and A82), C site (A180 and L181), D site (A184 and L188), E site (A328 and A330) and F site (I263); while the 10 active-site residues of P450cam including F87 (A site), Y96 and F98 (B site), L244 and V247 (C site), V295 and D297 (D site), I395 and V396 (E site), and T101 (F site) were selected for CAST (Figure 3A and B). Essentially, all these residues have been identified to be relevant to the activity and selectivity of these two P450 enzymes (Bell et al., 2003a; Bell et al., 2003b; Manchester and Ornstein, 1996; Zeymer and Hilvert, 2018). Grouping the active-site residues into six sites could maximize the cooperative effects with minimal screening efforts. To lower the screening numbers, the NDT codon degeneracy was adopted, which would theoretically give 100% and 85% coverage for the one- and two-residue(s) containing mutation sites, respectively (Reetz et al., 2008). Following this design, two P450 libraries, each of which contained 2,016 mutants of P450 BM3* and P450cam, were constructed using the complementary primers (Table S1 in Supporting Information) that carry the differentially saturated mutations. All these P450 mutants were organized into twelve sublibraries (i.e., P450 BM3* A–F and P450cam A–F) according to their mutation sites.

High-throughput screening

In the 96-well plate-based screening, each individual cell lysates of the P450 BM3* and P450cam (that was co-expressed with its redox partners Pdx/PdR) mutants from the corresponding sublibraries were mixed in the same well that pre-contained a solution of the mixed seven substrates **1**–**7** and NAD^+/$NADP^+$/glucose/glucose dehydrogenase (GDH) to supply P450s with the recycled reducing equivalents. Upon the reactions of the two distinct P450s with the mixed seven substrates in a single well (as shown in Figure 1C; rather than only one reaction of a single mutant with one substrate in normal DE setting as shown in Figure 1A), which in principle mimicking the complex natural cellular enzymatic reactions (Figure 1B), the reaction mixtures were extracted with ethyl acetate and the extracts were analyzed by GC since there lacks a convenient colorimetric or fluorometric method to detect the oxidative products of **1**–**6**. In this regard, the two colored products of **7** (Figures S1 and S4 in Supporting Information) could act as visible indicators for the varied activities of P450 mutants.

From the 2,016 chromatograms carrying the reactivity

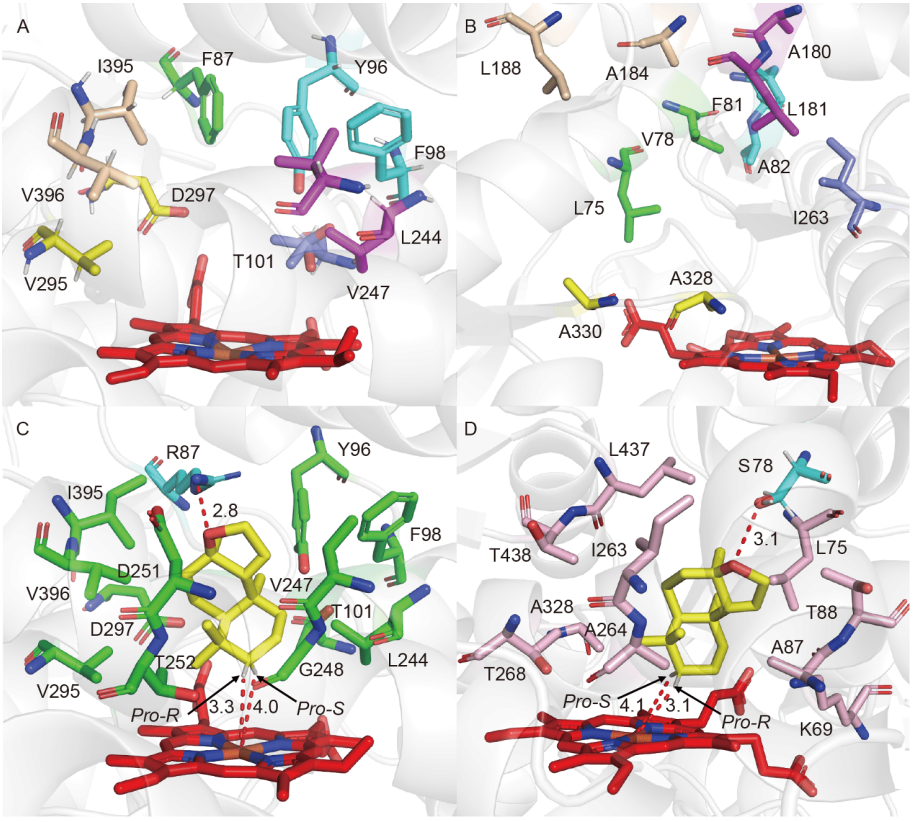

Figure 3 Structural analysis of P450cam and P450 BM3* variants. A, The selected mutational sites of P450cam (PDB ID code: 2ZWU). B, The selected mutagenesis sites of P450 BM3* (PDB ID code: 2X80). The key amino acids grouped into six sites are shown as sticks with different colors. C, The ideal Autodock pose of **5** in P450cam (PDB ID code: 1RF9): the key **5**-interacting amino acids with F87 replaced by an arginine *in silico* are shown as sticks. D, The ideal Autodock pose of **5** in P450 BM3* (PDB ID code: 2X7Y): the key **5**-interacting amino acids with V78 replaced by a serine *in silico* are shown as sticks. The heme group is shown as stick in red with the central iron atom in orange. The substrate **5** is shown as stick in yellow. The R87 in (C) and S78 in (D) that result in the convergent functionality of 3β-hydroxylation of **5** are highlighted in cyan. The distances from the C–H bonds to the heme-iron reactive center in angstroms are indicated by the dashed lines.

information of 28,224 reactions, any P450-catalyzed conversions could be readily detected by consumption of one or more substrate(s) and generation of corresponding product(s) (Figure S4 in Supporting Information). For all the mixed reactions that displayed higher substrate conversion rates than those of either starting P450 enzymes, we performed deconvolution to identify the exact paring of the specific mutant enzyme and the reacted substrate(s) in a one-P450-against-one-substrate (1P×1S) manner, and the active reactions were further confirmed by GC-MS analysis. For all the P450 mutants responsible for improved conversions, their mutation sites were determined by DNA sequencing. Of note, under the screening conditions, wild-type P450cam was only able to recognize **1** (as native substrate), and entirely inactive towards **2**–**7**; while P450 BM3* showed better substrate flexibility since it could oxidize **2**–**4** to different extent, but was unable to transform **1** and **5**–**7** (Figure 4 and Table 1).

Compared to the normal 1P×1S DE, the 2P×7S DE approach enhanced the throughput of screening for 14 times within a given time. Complete GC analysis of 2,016 samples containing 28,224 reactions (Figure 4) revealed an extraordinarily high hit rate of 68.1% (a well with any reaction showing a higher substrate conversion ratio than either P450 BM3* or wild-type P450cam was defined as a "hit") and distinct reactivity patterns towards different substrates. For instance, none of the tested mutants showed any activity against **6**; while many P450 variants in sublibraries A, B and C demonstrated increased activities towards **3** (Table 1). In particular, several mutants from sublibrary E of P450 BM3*, including A328F/A330F, A328F/A330Y, A328N/A330N, A328N/A330Y, A328N/A330C, A328N/A330F and A328N/A330L showed significantly improved selectivity for 2,3-epoxy-geraniol (**3a**, Figures S5 and S6 in Supporting Information). Comparatively, the hit rates of P450 BM3* were 100.0%, 100.0%, 10.3% and 99.1% higher than those of P450cam toward **3**, **4**, **5** and **7**, respectively. The only exception was **1**, towards which P450cam showed a 66.7% higher hit rate than P450 BM3*. Regarding the mutation sites, the hits of both P450 BM3* and P450cam mainly belonged to the corresponding sublibraries A–C for substrates **1**–**5**. For **7**, sublibraries C–E of P450 BM3* generated more

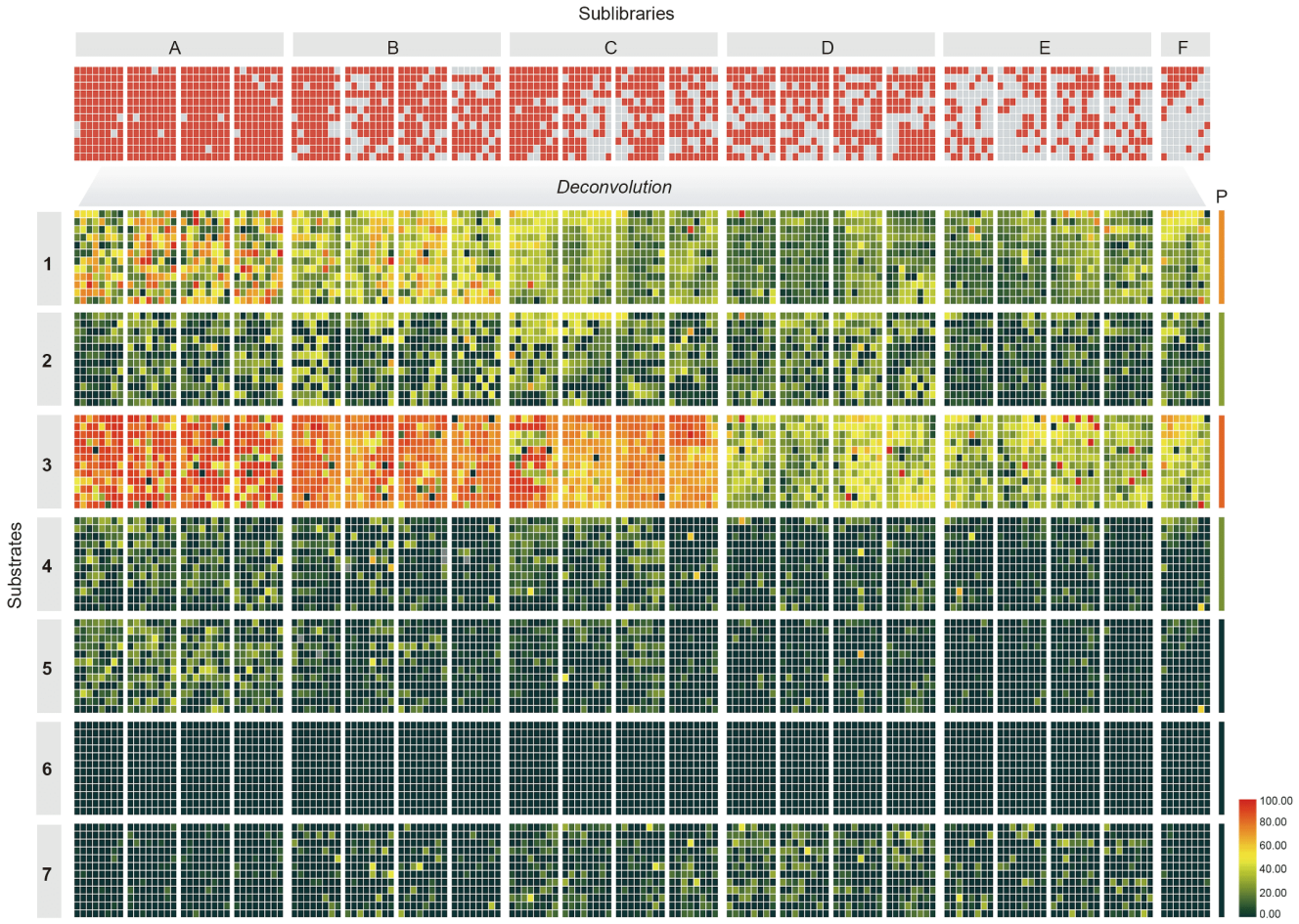

Figure 4 Substrate conversion rates of the whole P450 mutant library. As shown in the upper panel, the whole library including 2,016 P450 BM3* mutants of A–F sublibraries and 2,016 P450cam variants of A–F sublibraries were arranged in twenty-one 96-well microtiter plates with each individual well containing one P450 BM3* mutant, one P450cam mutant (together with the co-expressed Pdx/PdR), seven mixed substrates (**1**–**7**) and NAD^+/$NADP^+$/glucose/GDH for cofactor recycling. The "hit" and inactive reactions are colored in red and grey, respectively. In the lower panel, the GC analytic data for the 2,016 mixed reaction samples were devonvoluted to 28,224 reactivity results of the individually mixed P450 BM3* and P450cam mutants. Two parallel reactions catalyzed by the two mixed parental P450s under the same reaction conditions were carried out as controls. The substrate conversion rates of the control reactions catalyzed by parental enzymes are shown separately in the rightmost panel as marked by "P". The color codes in the heat map indicate the differential substrate conversion ratios.

Table 1 P450 variants in the combined sublibraries A–F that showed better substrate conversions than either parental enzymes towards seven substrates[a)]

Substrate	P (%)	A	B	C	D	E	F	Total hits	Hit rate (%)
1	73.9	62	11	2	1	3	1	80	4.0
2	28.6	48	105	112	89	22	13	389	19.3
3	82.8	239	135	65	4	11	1	455	22.6
4	23.9	54	31	44	17	5	8	159	7.9
5	0	265	150	164	112	64	24	779	38.6
6	0	0	0	0	0	0	0	0	0
7	0	72	78	181	183	106	5	625	31.0

a) "P" stands for the substrate conversion rates of the control reactions catalyzed by the mixed parental enzymes.

hits than other sublibraries (Table S2 in Supporting Information).

Taken together, these above results indicate that (i) P450 BM3* is probably a better starting P450 template than P450cam for DE in general due to the better substrate flexibility and higher hit rate; (ii) the mutation sites should be carefully selected for different substrates (even for those in the same structural class, e.g., terpenoids tested in this study); otherwise it may be difficult or even impossible to gain active mutants (e.g., the inappropriate selection of

mutation sites might have failed the screening on **6**); (iii) the selection pressure (the total screening number, mutation rate, substrate properties, etc.) needs to be adjusted according to the challenge level of the target reaction, which could be evaluated by the thermodynamic nature of the reaction, the matching/compatibility between the substrate and the active-site predicted by molecular docking and/or the published mutational data, and the new reactivity data collected from more practices of the current MEMS DE strategy; and (iv) mutagenesis at different sites could enable the same reaction, highlighting that an enzyme could find different solutions for a common catalytic goal.

Of particular interest, a number of isoenzymes (i.e., the functionally identical enzymes with different evolutionary origins) were evolved from P450 BM3* and P450cam during the 2P×7S DE, demonstrating intriguing events of convergent evolution in laboratory. These isoenzymes included (i) P450 BM3* A82F, A180I/L181F, A180F/L181V, A180Y/L181F, A180R/L181H, A184N/L188N, A184I/L188Y, A184N/L188H, A184N/L188F, A184N/L188Y, A184N/L188S, A328F/A330F, and A328L/A330I and P450cam Y96N for **7** oxidation (Figure S1 and Table S2 in Supporting Information); and (ii) P450 BM3* V78S, L75I/V78C, L75F/V78I, L75N/V78S, and L75I/V78S and P450cam F87R, F87K, and F87H for 3*β*-hydroxylation of **5** to form 3*β*-OH-ambroxide (**5a**) (see Figures S5, S7 and S8 in Supporting Information for structural determination data). Further oxidation of **5a** into the keto product **5b** (Figures S5 and S9 in Supporting Information**)** to different extent was also observed under the 1P×1S condition.

Interestingly, all P450 BM3*-derived ambroxide 3*β*-hydroxylases including V78S, L75F/V78I, L75I/V78S and L75N/V78S contain an amino acid substitution at V78, indicating that this position is crucial for productive binding of **5**. Thus, we performed saturation mutagenesis at V78 and the V78S mutant displayed the highest 3*β*-hydroxylation activity towards **5** among the 20 variants (Figure 5A). Of note, the mutant V78G mainly catalyzed the oxidation at the C12 position, giving rise to 12-OH-amboxide (**5c**) and sclareolide (**5d**) (Figure 2, Figures S5 and S10 in Supporting Information). Moreover, the introduction of an additional amino acid substitution at the position of L75 improved the selectivity of 3*β*-hydroxylation since the further oxidation of **5a** to **5b** (Figure 5C, Figures S5 and S9 in Supporting Information) was inhibited probably due to the significantly attenuated binding of **5a** to the mutants containing the L75 modification. For P450cam-derived ambroxide 3*β*-hydroxylases, we analyzed the most active variant F87R, whose substrate conversion rate was 68% higher than that of the wild type P450cam. Further saturation mutagenesis analysis showed that the first three places mutants were F87R, F87K and F87H (Figure 5B), which is consistent with the screening results, further supporting the validity of our MEMS DE strategy.

Autodock analysis of the two ambroxide 3*β*-hydroxylases

To understand how P450cam F87R and P450 BM3* V78S share the common substrate specificity and catalytic selectivity, we used AutoDock 4.2 to explore the binding mode of **5** with these two proteins. The F87R mutation was introduced into the structure of P450cam (PDB ID code: 1RF9) *in silico* and the mutated protein was utilized as a template for creating the starting coordinates. In the top 10 lowest energy docking solutions, we found one ideal catalytic conformation of P450cam F87R. The replacement of F87

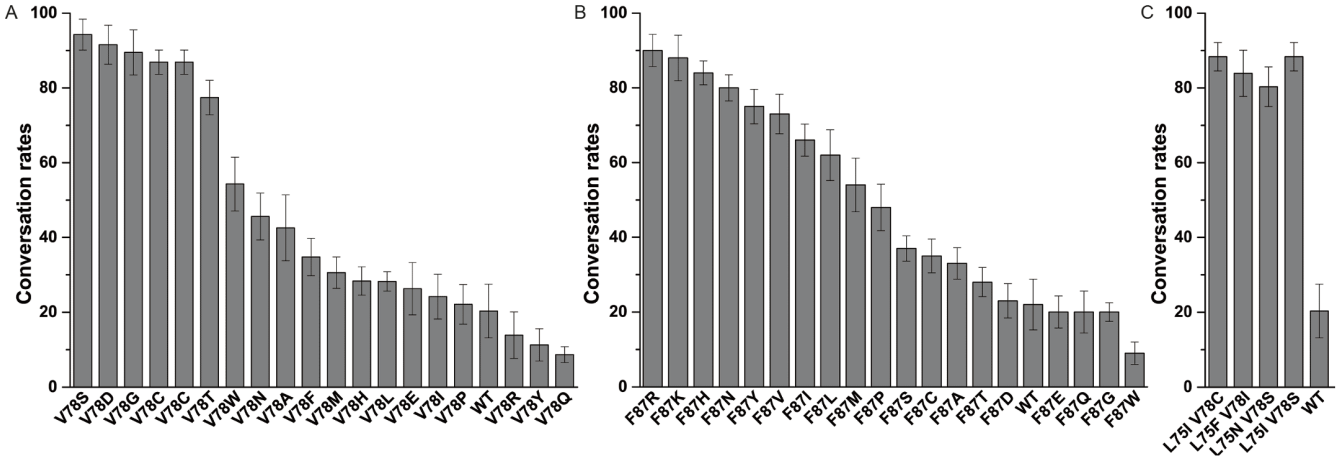

Figure 5 Mutagenesis analysis. A, The conversion rates of **5** by twenty V78 variants of P450 BM3*. B, The conversion rates of **5** by twenty F87 variants of P450cam. C, The conversion rates of **5** by three L75/V78 double mutants of P450 BM3*. The substrate conversion rates were calculated by $(1-AUC_{unreacted\ substrate}/AUC_{total\ substrate})\times100\%$ ($AUC_{total\ substrate}$ was derived from the control reaction using boiled enzyme under the identical reaction conditions); AUC: area under curve of the GC ion count chromatograms. All the experiments were carried out in triplicate. The reaction conditions: 0.5 mmol L^{-1} **5**, 2 μmol L^{-1} P450 enzyme (2 μmol L^{-1} Pdx and 2 μmol L^{-1} PdR were supplemented for P450cam), and 500 μmol L^{-1} NADH (for P450cam) or 500 μmol L^{-1}

with an arginine leads to the formation of a key hydrogen bond between the guanidine group and the only oxygen atom in **5** (Figure 3C). The specific anchoring-like interaction determines the substrate position/orientation in the active-site, thereby presenting the *pro*-3*R* C–H bond to be hydroxylated towards the heme-iron reactive center with the distance of 3.3 Å (*versus* 4.0 Å for the *pro*-3*S* C–H bond). This explains the regio- and stereoselectivity of 3*β*-hydroxylation by this mutant enzyme. Superimposition of the structure 1RF9 and the published P450cam-**1** complex structure (PDB ID code: 2ZWU) further revealed that R87 would provide extra space for the bigger substrate **5** (than **1**) with its side chain pointing away from the heme group (Figure S11 in Supporting Information).

AutoDock was used again to explore the binding mode of **5** with P450 BM3* V78S. The V78S mutation was introduced into the structure of P450 BM3* (PDB ID code: 2X7Y) *in silico* and the resulted mutant was used as the template. Similarly, in the top 10 lowest energy docking solutions, we selected one ideal catalytic conformation, in which the *pro*-3*R* C–H bond to be oxidized is 3.1 Å (*versus* 4.1 Å for the *pro*-3*S* C–H bond) away from the heme-iron reactive center and the orientation of this C–H bond in substrate is consistent with the experimentally observed stereoselectivity (Figure 3D). The modeling of the complex revealed that **5** mainly through hydrophobic interactions binds to P450 BM3* V78S via K69, L75, S78, A87, T88, I263, A264, T268, A328, and T438 (Figure 3D). Interestingly, the V-to-S mutation enables a hydrogen bond to be built between the OH group of serine and the heteroatom in **5**. This anchoring strategy is analogous to the one adopted by P450cam F87R (Figure 3C and Figure S12 in Supporting Information).

DISCUSSION

Compound **5** is the most appreciated substitute for the endangered ambergris, which is widely used as a key component of perfume (Frija et al., 2011). Different ambroxide-type compounds are valuable synthetic targets in fragrance industry (Schalk et al., 2012). Thus, the P450 ambroxide 3*β*-hydroxylases derived from MEMS DE may hold significant application potential. Moreover, comparative mechanistic analysis of the isoenzymes of different P450 origins could provide new insights into P450 substrate binding/orientation mechanisms resulted from convergent evolution, which would benefit the future rational design of P450 enzymes.

Taking into account all the P450 BM3*- and P450cam-derived ambroxide 3*β*-hydroxylase mutants, the key mutations are all located in B′ helix, which is the most variable secondary-structure element among P450 families and acts as a flexible lid over the substrate binding pocket together with F/G loop (Sherman et al., 2006). It has been well-known that B′ helix is essential for substrate specificity determination in many P450s including P450 BM3* and P450cam (the B′ helices of these two prototypical P450s are quite different as shown in Figure S3 in Supporting Information). Thus, we suggest that the highly variable B′ helix might be an optimal spot of mutagenesis for substrate specificity engineering. Furthermore, for a hydrophobic substrate such as a terpenoid, the entropy gaining might be the major driving force for its binding to the usually hydrophobic substrate binding pocket of a P450 enzyme. This may explain why distinct P450 substrate binding pockets can acommodate common substrates as shown in Figure 3. However, the polar heteroaom(s) (e.g., the sole oxygen atom in **5**) could be essential to determine the binding mode/orientation through more specific substrate-enzyme interactions. Our docking results (Figure 3C and D) support such a substrate binding/orientation strategy. More detailed mechanistic understanding of this strategy depends on resolution of the co-crystal structures of the P450 BM3*- and P450cam-derived ambroxide 3*β*-hydroxylases in complex with **5**, which requires more efforts and is currently ongoing in this laboratory.

In this work, we established the proof-of-concept of a novel MEMS DE model. This simple but effective strategy improved both screening efficiency and hit rate by mimicking NE that is more “violent and chaotic” than conventional DE. Since the HTSs based on survival selection or the fast colorimetric/fluorometric assays are often unavailable, MEMS DE is particularly useful for the screenings depending on “slow” analytic methods such as GC and LC. MEMS DE is also valuable for studying convergent evolution of proteins/enzymes. With no doubt, the data analysis of MEMS DE is more complicated than the conventional “one-protein-for-one-task” DE. However, it is worthwhile if considering the multiplication of screening throughput and hence the saving of time and cost on chromatographic analysis. It is also worth noting that the crossed inhibition effect (although not observed in this study) may occur in a MEMS DE approach, which is a potential drawback of this methodology. Nonetheless, this undesired effect could be overcome by a robust MEMS DE process provided that a substrate can be better recognized by the hit mutant enzyme than its competitive inhibitor. After all, NE of all enzymes is undergoing in such mixture circumstances.

In the pilot practice of MEMS DE for co-evolving P450 BM3* and P450cam, we witnessed a series of convergent evolution events in laboratory. In particular, a number of efficient and selective ambroxide 3*β*-hydroxylases including the P450 BM3* V78 variants and P450cam F87 mutants were discovered. Inspired by the different solutions of isoenzymes for a common P450 reaction, designing an anchoring residue in B′ helix region to lock the heteroatom in a hydrophobic substrate could be developed into a general strategy for P450 enzyme engineering. More importantly, we envision that the

broader application of the MEMS DE strategy for a larger repertoire of enzymes in the future will not only provide more high-quality enzymes on-demand in a more efficient manner, but also accumulate much more mutagenesis data for rational design of enzymes on the basis of the big data demanding methodologies including machine learning and artificial intelligence.

MATERIALS AND METHODS

Materials

Antibiotics and chemicals were purchased from SolarBio (Beijing, China) and Sigma-Aldrich (USA). KOD-Plus Neo DNA Polymerase was obtained from TOYOBO (Japan). Restriction enzymes were bought from TaKaRa (Dalian, China). The kits for plasmid extraction and DNA purification were purchased from OMEGA Bio-Tek (USA) and Promega (USA). His-tagged protein purification used Qiagen Ni-NTA resin (USA), Millipore Amicon Ultra centrifugal filters (USA), and PD-10 desalting columns from GE Healthcare (USA). Oligonucleotides synthesis and DNA sequencing were conducted by Sangon Biotech (Shanghai, China).

General experimental procedures

The UV-visible spectra were taken on a Spectrophotometer Infinite M200 Pro (Tecan Group Ltd., Switzerland). Pre-coated silica gel plates (GF254, Qingdao Marine Chemical Inc., Qingdao, China) were used for TLC analysis and preparations. Silica gel (200–300 mesh, Qingdao Marine Chemical Inc.) was used for column chromatography. GC and GC-MS analyses were carried out using Agilent 7980B and 1200 series instruments (Agilent Technologies Inc., USA) with an Agilent HP-5 column (30 m×0.25 mm, 2.5 μm). The program used for GC analysis was as follows: the temperature was increased from 50°C to 260°C at 10°C min^{-1}, and maintained at 260°C for 8 min. LC-quadrupole time-of-flight mass spectrometry (LC-Q-TOF/MS) analysis was performed on a maXis UHR-TOF system (Bruker BioSpin GmbH Co., Germany) using a Thermo Scientific Hypersil GOLD column (5 μm, 2.1 mm×100 mm, Thermo Fisher Scientific Inc., USA). Nuclear magnetic resonance (NMR) spectra were acquired on a Bruker 600 MHz spectrometer (Bruker BioSpin GmbH Co.). NMR data were processed using MestReNova software.

Construction of expression vectors

The DNA sequence of full-length P450 BM3* was cloned into pET30a between the *Bam*HI and *Hin*dIII restriction sites to afford pET30a-*bm3**. The expression vectors for P450cam and its redox partners Pdx/PdR were constructed as described previously (Zhang et al., 2018). For construction of the pCDFDuet-1-*pdx*-*pdR* co-expression vector, the *pdx* and *pdR* genes bearing corresponding restriction sites were PCR-amplified and sequentially inserted into the *Nde*I-*Bgl*II and *Eco*RI-*Not*I sites of pCDFDuet-1. The P450cam gene was inserted between the *Nde*I and *Hin*dIII restriction sites of pET30a to afford pET30a-*cam*. The plasmids pCDFDuet-1-*pdx*-*pdR* and pET30a-*cam* were co-transformed into *E. coli* resulting in the redox-sufficient P450cam biocatalysts. The plasmids pET30a-*bm3** and pET30a-*cam* were used as the templates for all the P450 BM3* and P450cam variants used in this study.

Library construction

Site-specific mutagenesis was performed using a modified QuikChange^{TM} mutagenesis protocol. Primers were designed based on the particular amino acid(s) chosen with NDT codon degeneracy (Table S1 in Supporting Information). The mutant libraries were constructed using overlap PCR with KOD-Plus Neo DNA Polymerase (TOYOBO). PCR products were analyzed on agarose gel by electrophoresis and purified using the Promega Wizard® SV Gel and PCR Clean-Up System. The recovered PCR products were digested with *Dpn*I at 37°C for 3 h to remove the template DNA, and then directly transformed into the electro-competent *E. coli* BL21 (DE3) cells to construct the mutant libraries.

Screening in 96-well plates

Single colonies were randomly picked and inoculated into 300 μL of LB medium containing 50 μg mL^{-1} kanamycin in a certain number of sterilized 96-deepwell plates. The cultures were grown at 37°C, 220 r min^{-1} for 12 h. The overnight culture (40 μL) in each well was transferred into a new sterilized 96-deepwell plate pre-containing 400 μL of TB medium (supplemented with 50 μg mL^{-1} kanamycin, 1 mmol L^{-1} thiamine, and the rare salt solution: 25 μmol L^{-1} $FeCl_3·6H_2O$, 4 μmol L^{-1} $ZnCl_2$, 2 μmol L^{-1} $CoCl_2·6H_2O$, 2 μmol L^{-1} $Na_2MoO_4·2H_2O$, 2 μmol L^{-1} $CaCl_2$, 3 μmol L^{-1} $CuSO_4$ and 2 μmol L^{-1} H_3BO_3). This plate was incubated at 37°C, 220 r min^{-1} for 4 h. Then, the P450 enzyme expression was induced by the addition of 0.2 mmol L^{-1} isopropyl-*β*-D-thiogalactopyranoside (IPTG) and 0.5 mmol L^{-1} 5-aminolevulinic acid (final concentrations) into each individual wells and conducted at 20°C, 230 r min^{-1} for 20 h. The cells were pelleted by centrifugation at 3,700×*g* for 10 min and stored at 80°C for later use. The freeze-thaw cell pellets were re-suspended in 50 mmol L^{-1} potassium phosphate buffer (pH 7.4) (200 μL per well) containing 100 mg L^{-1} lysozyme, 300 U mL^{-1} DNase I and 10% Triton X-100. The 96-well plates were centrifuged and the supernatants were transferred to a new microtiter 96-well plate, to which 2.8 mmol L^{-1} of

mixed substrates **1**–**7** (0.4 mmol L^{-1} for each substrate), 0.5 mmol L^{-1} NADPH and NADH as electron donors for P450 BM3* and P450cam respectively, and 20 mmol L^{-1} glucose/5 U GDH as an NAD(P)H regeneration system were added. The plates were incubated at 30°C for 16 h, after which the reactions were quenched by adding 300 μL of ethyl acetate, and the mixtures were shaken at 37°C for 30 min for organic extraction. The mixtures were centrifuged at 3,700×*g* for 10 min and the organic phases were directly used as samples for GC or GC-MS analysis with a HP-5 column.

Protein expression and purification

A single colony of transformant was inoculated into LB medium containing 50 mg L^{-1} kanamycin. The overnight seed culture was used for 1:100 inoculation of 0.5 L TB medium containing 50 mg L^{-1} kanamycin, 1 mmol L^{-1} thiamin, and the rare salt solution. The *E. coli* cells were grown at 37°C for 2–3 h until A_{600} reached 0.4–0.6, at which IPTG was added to a final concentration of 0.2 mmol L^{-1} to induce gene expression, and 0.5 mmol L^{-1} 5-aminolevulinic acid was supplemented as the heme synthetic precursor. The cells were cultured at 20°C for another 20 h. The culture was centrifuged at 6,000×*g* for 10 min to pellet cells. The following protein purification was carried out by following the previously developed procedure (Xue et al., 1998; Du et al., 2017). Purified proteins were flash-frozen by liquid nitrogen and stored at −80°C for later use.

Enzyme concentration determination

P450 BM3* and P450cam were purified according to the procedures described previously (Boddupalli et al., 1990; Poulos et al., 1987). The functional P450 concentrations were determined from CO-reduced difference spectra (Guengerich et al., 2009) using the extinction coefficient of $\varepsilon_{450-490}$=91,000 M^{-1} cm^{-1}. The concentrations of ferredoxin and ferredoxin reductase were determined by measuring the absorbance at the selected wavelengths. The extinction coefficients used for calculation of concentrations were ε_{391}=102,000 M^{-1} cm^{-1} for Pdx and ε_{455}=10,400 M^{-1} cm^{-1} for PdR (Gunsalus and Wagner, 1978).

Structural determination of products

Products **3a**, **5a** and **5b** were isolated from the *in vitro* enzymatic reactions with purified proteins. Compounds were separated by silica gel column using a linear mobile phase gradient of petroleum ether/ethyl acetate and eluted with 13:1 (**3a**), 9:1 (**5a**) and 10:1 (**5b**) of petroleum ether/ethyl acetate (*v*/*v*). The products were characterized by ^{1}H NMR using $CDCl_3$ as solvent on a Bruker Avance III 600 MHz spectrometer with a 5 mm TCI cryoprobe. Chemical properties of **3a**, **5a** and **5b** are as follows: Compound **3a**: colorless oil; $[\alpha]_D$=−9.09 (*c* 2.6, in CH_2Cl_2); HR-ESI-MS *m*/*z* 171.1378 $[M+H]^+$ (*calc*. 171.1385); ^{1}H NMR (600 MHz, $CDCl_3$): δ 5.08 (t, *J*=6.5 Hz, 1H), 3.83 (dd, *J*=12.1, 4.2 Hz, 1H), 3.68 (dd, *J*=12.1, 6.7 Hz, 1H), 2.97 (dd, *J*=6.6, 4.3 Hz, 1H), 2.08 (m, 2H), 1.68 (s, 3H), 1.71–1.65 (m, 1H), 1.61(s, 3H), 1.50–1.44 (m, 2H), 1.30 (s, 3H). The ^{1}H NMR spectrum of **3a** is consistent with that of 2,3-epoxy-geraniol (Egami et al., 2010). Compound **5a**: white powder; HR-ESI-MS *m*/*z* 253.2169 $[M+H]^+$ (*calc*. 253.2168), ^{1}H NMR (600 MHz, $CDCl_3$): δ 3.94–3.89 (m, 1H), 3.83 (q, *J*=8.2 Hz, 1H), 3.25 (dd, *J*=11.1, 5.2 Hz, 1H), 1.09 (s, 3H), 1.00 (s, 3H), 0.85 (s, 3H), 0.80 (s, 3H). The configuration of the P450-installed hydroxyl group was deduced by comparing the *J* value of H-3 with that of the reported *ent*-3-hydroxyambroxide (García-Granados et al., 1999). Compound **5b**: white powder; HR-ESI-MS *m*/*z* 251.2014 $[M+H]^+$ (*calc*. 251.2011), ^{1}H NMR (600 MHz, $CDCl_3$): ^{1}H NMR (600 MHz, $CDCl_3$) δ 3.97 (dd, *J*=13.4, 7.7 Hz, 1H), 3.88 (dd, *J*=16.5, 8.2 Hz, 1H), 2.65–2.57 (m, 1H), 2.49 (ddd, *J*=16.3, 7.5, 3.5 Hz, 1H), 2.05–1.98 (m, 1H), 1.86–1.78 (m, 3H), 1.77–1.72 (m, 1H), 1.66–1.59 (m, 2H), 1.56–1.43 (m, 3H), 1.16 (s, 3H), 1.14 (s, 3H), 1.08 (s, 3H), 0.98 (s, 3H).

AutoDock

The F87R and V78S mutations were introduced into P450cam (PDB ID code: 1RF9) and P450 BM3* (PDB ID code: 2X7Y) by Wincoot, respectively. Substrate **5** was docked into the structures of P450cam F87R and P450 BM3* V78S in the zwitterionic form using AutoDock 4.2 (Morris et al., 2009). Regents and water molecules were removed before docking. All side chains were set as rigid body and grid spacing was set to 0.5 Å. Other parameters remained as their default values. The top 10 lowest energy docking poses of substrate **5** from 2,500,000 searching results were selected, among which the ideal catalytic conformations were used for analysis.

Compliance and ethics *The author(s) declare that they have no conflict of interest.*

Acknowledgements *This work was supported by the National Key Research and Development Program of China (2019YFA0706900), the National Natural Science Foundation of China (32025001, 31872729, 31600045, 32071266, 31800664, 82022066, and 31800041), the Natural Science Foundation of Shandong Province, China (ZR2019ZD20, ZR2016CQ05, and ZR2019QC009), the Laboratory for Marine Drugs and Bioproducts of Pilot National Laboratory for Marine Science and Technology (Qingdao) (LMDBKF-2019-01), the Tianjin Synthetic Biotechnology Innovation Capability Improvement Project (TSBICIP-KJGG-001), the State Key Laboratory of Bio-organic and Natural Products Chemistry (SKLBNPC18242), the Fundamental Research Funds of Shandong University (2019GN030 and 2019GN033), and the Foundation of Qilu Uni-*

versity of Technology of Cultivating Subject for Biology and Biochemistry (No. 202014). We would like to thank Zhifeng Li, Jing Zhu and Jingyao Qu from the State Key laboratory of Microbial Technology of Shandong University for help and guidance in GC-MS and HRMS analysis.

References

Ahalawat, N., and Mondal, J. (2018). Mapping the substrate recognition pathway in cytochrome P450. J Am Chem Soc 140, 17743–17752.

Alcalde, M., Farinas, E.T., and Arnold, F.H. (2004). Colorimetric high-throughput assay for alkene epoxidation catalyzed by cytochrome P450 BM-3 variant 139-3. J Biomol Screen 9, 141–146.

Arnold, F.H., Wintrode, P.L., Miyazaki, K., and Gershenson, A. (2001). How enzymes adapt: lessons from directed evolution. Trends Biochem Sci 26, 100–106.

Bell, S.G., Chen, X., Xu, F., Rao, Z., and Wong, L.L. (2003a). Engineering substrate recognition in catalysis by cytochrome $P450_{cam}$. Biochem Soc Trans 31, 558–562.

Bell, S.G., Chen, X., Sowden, R.J., Xu, F., Williams, J.N., Wong, L.L., and Rao, Z. (2003b). Molecular Recognition in (+)-α-pinene oxidation by cytochrome $P450_{cam}$. J Am Chem Soc 125, 705–714.

Boddupalli, S.S., Estabrook, R.W., and Peterson, J.A. (1990). Fatty acid monooxygenation by cytochrome P-450BM-3. J Biol Chem 265, 4233–4239.

Brandenberg, O.F., Chen, K., and Arnold, F.H. (2019). Directed evolution of a cytochrome P450 carbene transferase for selective functionalization of cyclic compounds. J Am Chem Soc 141, 8989–8995.

Chen, Z.H., Zhang, S.X., Long, N., Lin, L.S., Chen, T., Zhang, F.P., Lv, X. Q., Ye, P.Z., Li, N., and Zhang, K.Z. (2016). An improved substrate cocktail for assessing direct inhibition and time-dependent inhibition of multiple cytochrome P450s. Acta Pharmacol Sin 37, 708–718.

Du, L., Dong, S., Zhang, X., Jiang, C., Chen, J., Yao, L., Wang, X., Wan, X., Liu, X., Wang, X., et al. (2017). Selective oxidation of aliphatic C–H bonds in alkylphenols by a chemomimetic biocatalytic system. Proc Natl Acad Sci USA 114, E5129–E5137.

Egami, H., Oguma, T., and Katsuki, T. (2010). Oxidation catalysis of Nb (salan) complexes: asymmetric epoxidation of allylic alcohols using aqueous hydrogen peroxide as an oxidant. J Am Chem Soc 132, 5886–5895.

Follmer, A.H., Mahomed, M., Goodin, D.B., and Poulos, T.L. (2018). Substrate-dependent allosteric regulation in cytochrome P450cam (CYP101A1). J Am Chem Soc 140, 16222–16228.

Frija, L.M.T., Frade, R.F.M., and Afonso, C.A.M. (2011). Isolation, chemical, and biotransformation routes of labdane-type diterpenes. Chem Rev 111, 4418–4452.

García-Granados, A., Martínez, A., Quirós, R., and Extremera, A.L. (1999). Chemical-microbiological semisynthesis of *enantio*-Ambrox® derivatives. Tetrahedron 55, 8567–8578.

Glieder, A., and Meinhold, P. (2003). High-throughput screens based on NAD(P)H depletion. In: Arnold, F.H., and Georgiou, G., eds. Directed Enzyme Evolution. Methods in Molecular Biology™. New York: Humana Press. 157–170.

Guengerich, F.P., Martin, M.V., Sohl, C.D., and Cheng, Q. (2009). Measurement of cytochrome P450 and NADPH-cytochrome P450 reductase. Nat Protoc 4, 1245–1251.

Gunsalus, I.C., and Wagner, G.C. (1978). Bacterial $P\text{-}450_{cam}$ methylene monooxygenase components: cytochrome *m*, putidaredoxin, and putidaredoxin reductase. In: Methods in Enzymology. New York: Academic Press. 166–188.

Haines, D.C., Tomchick, D.R., Machius, M., and Peterson, J.A. (2001). Pivotal role of water in the mechanism of P450BM-3. Biochemistry 40, 13456–13465.

Jung, S.T., Lauchli, R., and Arnold, F.H. (2011). Cytochrome P450: taming a wild type enzyme. Curr Opin Biotech 22, 809–817.

Li, Z., Jiang, Y., Guengerich, F.P., Ma, L., Li, S., and Zhang, W. (2020). Engineering cytochrome P450 enzyme systems for biomedical and biotechnological applications. J Biol Chem 295, 833–849.

Manchester, J.I., and Ornstein, R.L. (1996). Rational approach to improving reductive catalysis by cytochrome $P450_{cam}$. Biochimie 78, 714–722.

Markel, U., Essani, K.D., Besirlioglu, V., Schiffels, J., Streit, W.R., and Schwaneberg, U. (2020). Advances in ultrahigh-throughput screening for directed enzyme evolution. Chem Soc Rev 49, 233–262.

Morlock, L.K., Böttcher, D., and Bornscheuer, U.T. (2018). Simultaneous detection of NADPH consumption and H_2O_2 production using the Ampliflu™ Red assay for screening of P450 activities and uncoupling. Appl Microbiol Biotechnol 102, 985–994.

Morris, G.M., Huey, R., Lindstrom, W., Sanner, M.F., Belew, R.K., Goodsell, D.S., and Olson, A.J. (2009). AutoDock4 and AutoDockTools4: Automated docking with selective receptor flexibility. J Comput Chem 30, 2785–2791.

Myers, W.K., Lee, Y.T., Britt, R.D., and Goodin, D.B. (2013). The conformation of $P450_{cam}$ in complex with putidaredoxin is dependent on oxidation state. J Am Chem Soc 135, 11732–11735.

Narhi, L.O., and Fulco, A.J. (1987). Identification and characterization of two functional domains in cytochrome P-450BM-3, a catalytically self-sufficient monooxygenase induced by barbiturates in *Bacillus megaterium*. J Biol Chem 262, 6683–6690.

Ortiz de Montellano, P.R. (2015). Cytochrome P450: Structure, Mechanism, and Biochemistry. Fourth ed. Switzerland: Springer International Publishing.

Poulos, T.L., Finzel, B.C., and Howard, A.J. (1987). High-resolution crystal structure of cytochrome P450cam. J Mol Biol 195, 687–700.

Prier, C.K., Zhang, R.K., Buller, A.R., Brinkmann-Chen, S., and Arnold, F. H. (2017). Enantioselective, intermolecular benzylic C–H amination catalysed by an engineered iron-haem enzyme. Nat Chem 9, 629–634.

Qi, F., Lei, C., Li, F., Zhang, X., Wang, J., Zhang, W., Fan, Z., Li, W., Tang, G.L., Xiao, Y., et al. (2018). Deciphering the late steps of rifamycin biosynthesis. Nat Commun 9, 2342.

Reetz, M.T., and Carballeira, J.D. (2007). Iterative saturation mutagenesis (ISM) for rapid directed evolution of functional enzymes. Nat Protoc 2, 891–903.

Reetz, M.T., Kahakeaw, D., and Lohmer, R. (2008). Addressing the numbers problem in directed evolution. Chembiochem 9, 1797–1804.

Romero, P.A., and Arnold, F.H. (2009). Exploring protein fitness landscapes by directed evolution. Nat Rev Mol Cell Biol 10, 866–876.

Sakurai, K., Shimada, H., Hayashi, T., and Tsukihara, T. (2009). Substrate binding induces structural changes in cytochrome P450cam. Acta Crystlogr F Struct Biol Cryst Commun 65, 80–83.

Schalk, M., Pastore, L., Mirata, M.A., Khim, S., Schouwey, M., Deguerry, F., Pineda, V., Rocci, L., and Daviet, L. (2012). Toward a biosynthetic route to sclareol and amber odorants. J Am Chem Soc 134, 18900–18903.

Sherman, D.H., Li, S., Yermalitskaya, L.V., Kim, Y., Smith, J.A., Waterman, M.R., and Podust, L.M. (2006). The structural basis for substrate anchoring, active site selectivity, and product formation by P450 PikC from *Streptomyces venezuelae*. J Biol Chem 281, 26289–26297.

Tee, K.L., and Schwaneberg, U. (2006). A screening system for the directed evolution of epoxygenases: importance of position 184 in P450 BM3 for stereoselective styrene epoxidation. Angew Chem Int Ed 45, 5380–5383.

Urban, P., Truan, G., and Pompon, D. (2014). High-throughput functional screening of steroid substrates with wild-type and chimeric P450 enzymes. Biomed Res Int 2014, 1–11.

Wang, B., Li, C., Dubey, K.D., and Shaik, S. (2015). Quantum mechanical/molecular mechanical calculated reactivity networks reveal how cytochrome P450cam and its T252A mutant select their oxidation pathways. J Am Chem Soc 137, 7379–7390.

Whitehouse, C.J.C., Bell, S.G., and Wong, L.L. (2012). $P450_{BM3}$ (CYP102A1): connecting the dots. Chem Soc Rev 41, 1218–1260.

Wong, T.S., Wu, N., Roccatano, D., Zacharias, M., and Schwaneberg, U. (2005). Sensitive assay for laboratory evolution of hydroxylases toward

aromatic and heterocyclic compounds. J Biomol Screen 10, 246–252.
Xu, H., Liang, W., Ning, L., Jiang, Y., Yang, W., Wang, C., Qi, F., Ma, L., Du, L., Fourage, L., et al. (2020). Directed evolution of P450 fatty acid decarboxylases via high-throughput screening towards improved catalytic Activity. Chemcatchem 12, 80–84.
Xue, Y., Wilson, D., Zhao, L., Liu, H., and Sherman, D.H. (1998). Hydroxylation of macrolactones YC-17 and narbomycin is mediated by the *pikC*-encoded cytochrome P450 in *Streptomyces venezuelae*. Chem Biol 5, 661–667.
Zeymer, C., and Hilvert, D. (2018). Directed evolution of protein catalysts. Annu Rev Biochem 87, 131–157.
Zhang, K., El Damaty, S., and Fasan, R. (2011). P450 fingerprinting method for rapid discovery of terpene hydroxylating P450 catalysts with diversified regioselectivity. J Am Chem Soc 133, 3242–3245.
Zhang, K., Shafer, B.M., Demars II, M.D., Stern, H.A., and Fasan, R. (2012). Controlled oxidation of remote sp3 C-H bonds in artemisinin via P450 catalysts with fine-tuned regio- and stereoselectivity. J Am Chem Soc 134, 18695–18704.
Zhang, R.K., Chen, K., Huang, X., Wohlschlager, L., Renata, H., and Arnold, F.H. (2019). Enzymatic assembly of carbon-carbon bonds via iron-catalysed sp3 C–H functionalization. Nature 565, 67–72.
Zhang, W., Liu, Y., Yan, J., Cao, S., Bai, F., Yang, Y., Huang, S., Yao, L., Anzai, Y., Kato, F., et al. (2014). New reactions and products resulting from alternative interactions between the P450 enzyme and redox partners. J Am Chem Soc 136, 3640–3646.
Zhang, W., Du, L., Li, F., Zhang, X., Qu, Z., Han, L., Li, Z., Sun, J., Qi, F., Yao, Q., et al. (2018). Mechanistic insights into interactions between bacterial class I P450 enzymes and redox partners. ACS Catal 8, 9992–10003.
Zhou, H., Wang, B., Wang, F., Yu, X., Ma, L., Li, A., and Reetz, M.T. (2019). Chemo- and regioselective dihydroxylation of benzene to hydroquinone enabled by engineered cytochrome P450 monooxygenase. Angew Chem Int Ed 58, 764–768.

SUPPORTING INFORMATION

The supporting information is available online at https://doi.org/10.1007/s11427-021-1994-1. The supporting materials are published as submitted, without typesetting or editing. The responsibility for scientific accuracy and content remains entirely with the authors.